Energy transfer photoproximity labelling in live cells using an organic cofactor

Leander B. Crocker,[a] Jan Vincent V. Arafiles,[a,#] Judith M. Müchler,[a,b,#] Max Ruwolt,[a] Kristin Kemnitz-Hassanin,[a] Kilian Roßmann,[a,b] Christian E. Stieger,[a] Fan Liu,[a] Christian P. R. Hackenberger[a,b,*]

[a] Leibniz-Forschungsinstitut für Molekulare Pharmakologie (FMP), Robert-Rössle-Strasse 10, 13125 Berlin, Germany

[b] Department of Chemistry, Humboldt Universität zu Berlin, Brook-Taylor-Straße 2, 12489 Berlin, Germany

[#] These authors contributed equally

*corresponding author: hackenbe@fmp-berlin.de

Abstract

Photocatalytic proximity labelling has recently emerged as a powerful tool to resolve a wide variety of biomolecular and cellular interactions. While the use of high-resolution probe species, such as diazirines, enables cell-surface protein labelling with nanometre precision by generating highly reactive intermediates, intracellular applications are limited either by the intrinsic toxicity of frequently employed photocatalysts or lower resolution when long-lived reactive intermediates are used. In this work, we describe the discovery and application of an organic flavin cofactor derivative, deazaflavin, capable of diazirine activation to form carbenes through triplet energy transfer and offers unparalleled biocompatibility. We demonstrate deazaflavin-diazirine energy transfer labelling (DarT-labelling) not only allows for targeted extracellular scenarios using antibody conjugates but, most importantly, for intracellular interactome mapping of cell-penetrating peptides (CPPs). We successfully mapped the localisation of two popular polyarginine CPPs and identified potential key membrane interactors. Furthermore, we showed the applicability of DarT-labelling over extended time by mapping the intracellular trafficking of a stable cyclic derivative to reveal its eventual exocytosis from the cell. We envision DarT-labelling has the unmet potential to enable detailed profiling of intracellular dynamics across diverse biological systems with unprecedented spatiotemporal control.

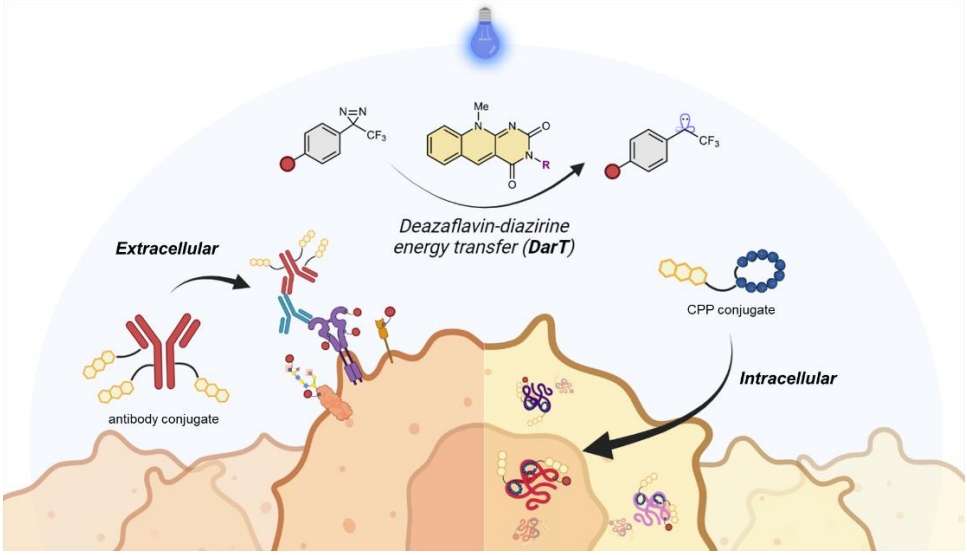

Introduction

Understanding biomolecular interactions in cellular functions is key to elucidating both life and disease mechanisms.[1] To achieve this, proximity-labelling (PL) methods have become powerful and diverse in their applicability to decipher protein, RNA and DNA interaction networks within living cells.[2,3] Mapping these interactions by PL has significantly benefitted from recent advances in mass-spectrometry (MS) to better understand disease pathology, discover novel biomarkers and therefore predict new therapeutic modalities.[4,5] Classical PL methods involve genetic fusion of an enzyme to a protein of interest (POI) to catalyse the generation of a reactive probe that labels proximal biomolecules. These methods, such as BioID (proximity-dependent biotin identification), have proven to be extremely valuable, but suffer from a lack of temporal control due to exogenous biotin treatment for extended periods.[6] Ascorbate peroxidase-based systems (APEX) offer faster labelling times but the H_2O_2 treatment required for generating reactive phenoxyl radicals for labelling results in cell death.[6] Photocatalytic proximity labelling or in short photoproximity labelling (PPL) has proven to be a useful alternative to such methods,[7,8] offering short labelling times, tuneable labelling radii,[9] long wavelength reactivity[10–12] and can even be applied *in vivo*.[13] In addition, photocatalytic enzymes such as mini Singlet Oxygen Generator (miniSOG)[14–17] and light-oxygen-voltage (LOV) domains[18] can be genetically incorporated into live cells; however, the fusion of an enzyme to a POI could alter the protein's natural structure, function and intracellular trafficking or obstruct potential biomolecular interactions.

Pioneering work by the groups of MacMillan, Oslund and Fadeyi introduced a Dexter energy transfer methodology in which a small molecule iridium photocatalyst activates a diazirine-based

probe to generate carbenes with a short half-life (2 ns) to enable microenvironment mapping (μMap) on cell surfaces.[19] Although highly efficient, the use of iridium photocatalysts in PPL is curtailed by material sustainability and cytotoxicity. As a result, approaches have emerged utilising organic PCs such as flavin,[20–22] acridinium and fluorescein derivatives[23–26] with great success and offer better suitability for intracellular PPL.[27] So far, subcellular compartments such as mitochondria[25,26] and nuclei[23,24] have been investigated by PPL taking advantage of the inherent cellular localisation of organic photocatalysts,[25] appendage of organelle targeting groups,[23,26] or protein tags.[24] However, these reports utilise longer half-life species such as phenoxyl radicals (≤ 1 ms),[28] nitrene-derived reactive intermediates (10 μs)[29] or $^1O_2$ (0.2 to 3 μs)[30,31] that do not offer the same resolution as carbenes. To the best of our knowledge, intracellular examples of carbene generation *via* energy transfer has been described using iridium photocatalysts for drug target identification[32] and stress granule interactome mapping,[33] but wider use of these catalysts for other PPL applications are hindered by intracellular cytotoxicity[32,34] and propensity for mitochondrial localisation.[35,36]

To overcome these limitations, we sought to identify a readily accessible organic photocatalyst with the following characteristics: i) efficient Dexter energy transfer with diazirines for high resolution PPL, ii) excellent biocompatibility and iii) spatiotemporal control over labelling. Herein, we report the discovery of a naturally occurring flavin cofactor analogue, deazaflavin,[37] capable of activating diazirines (as well as other major probes) *via* energy transfer in live-cells. Due to the catalyst's non-cytotoxicity and minimalist design, we were able to demonstrate both extra- and intracellular deazaflavin-diazirine energy transfer labelling (DarT-labelling) in live cells. This allowed us to elucidate the protein interactomes of polyarginine cell-penetrating peptides (CPPs) that relate to their uptake mechanism, localisation affinity and trafficking within the cell.

Results and Discussion

Deazaflavin discovery and characterisation

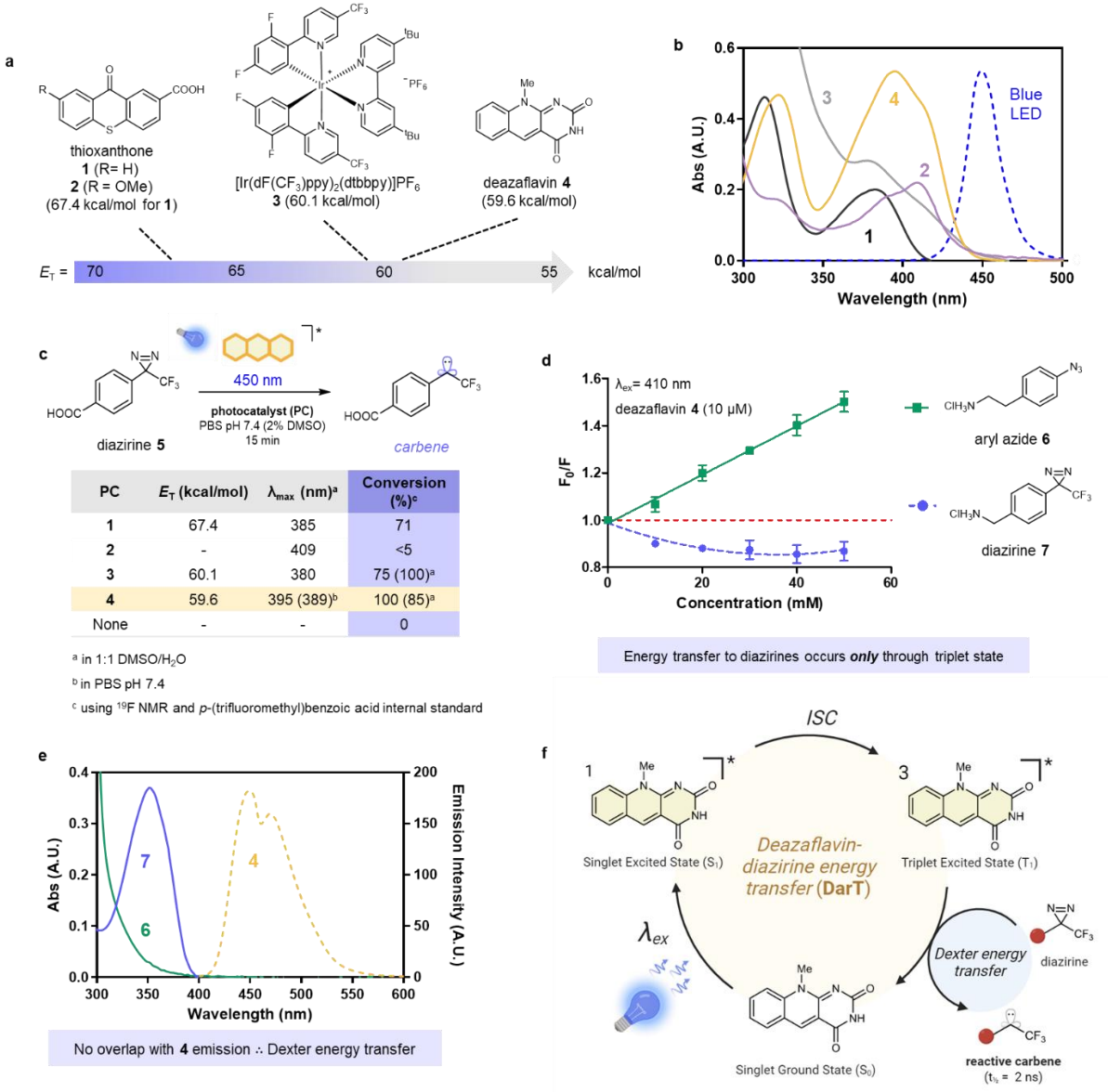

PC	E_T (kcal/mol)	λ_{max} (nm)[a]	Conversion (%)[c]
1	67.4	385	71
2	-	409	<5
3	60.1	380	75 (100)[a]
4	59.6	395 (389)[b]	100 (85)[a]
None	-	-	0

[a] in 1:1 DMSO/H_2O
[b] in PBS pH 7.4
[c] using ^{19}F NMR and *p*-(trifluoromethyl)benzoic acid internal standard

Fig. 1: Photocatalyst screening and mechanistic validation of energy transfer. a) Structures and triplet energies (E_T) of photocatalysts **1**-**4**. **b)** UV-Vis spectra of photocatalysts **1**-**4** (50 μM) in 1:1 DMSO/H_2O. **c)** Photocatalyst screening of blue light (450 nm) activation of diazirine **5** resulting in the discovery of deazaflavin **4** as the optimal energy transfer catalyst. **d)** Stern-Volmer fluorescence quenching plot of deazaflavin **4** (10 μM, λ_{ex} = 410 nm) with increasing concentrations of aryl azide **6** and diazirine **7** in 1:1 DMSO/H_2O (N_2 purged). **e)** UV-Vis spectra of aryl azide **6** and diazirine **7** (1 mM) vs deazaflavin fluorescence emission in PBS pH 7.4 (1% DMSO). **f)** Mechanism of deazaflavin-diazirine energy transfer (DarT).

We initially selected the well-known thioxanthones[38–40] as potential triplet energy sensitisers to activate diazirine **5** ($E_T \geq 60.1$ kcal/mol)[19] in PBS upon blue LED (450 nm) irradiation (**Fig. 1a** and **b**). Thioxanthone **1** (E_T = 67.4 kcal/mol),[41] provided good conversions (>70%) of diazirine **5** upon

irradiation for 15 min in PBS that is comparable with iridium catalyst **3**,[19] despite having almost no absorbance overlap with the incident photons (**1** λ_{max} = 385 nm, **Fig. 1b** and **Supplementary Fig. S1a**). Red-shifted photochemical reactivity relative to absorption spectra has been well-established and can therefore explain these observations.[42] Additionally, attempts to increase the blue light absorption of **1** through methoxy substitution (thioxanthone **2, Fig. 1a-b** and **Supplementary Fig. S1a**) resulted in severely diminished conversions of **5** (< 5%, **Fig. 1c**) most likely due to lowering the excited triplet energy.[41] Due to poor solubility in PBS, iridium **3** did not provide complete conversion of **5** (75%) but was highly efficient in 1:1 DMSO/H_2O (**Fig. 1c**).

We next turned our attention the high triplet energy flavin derivative, deazaflavin **4** (E_T = 59.6 kcal/mol)[43] and observed complete conversion of **5** after 15 min blue LED irradiation in PBS by ^{19}F NMR (**Fig. 1c** and **Supplementary Fig. S2**). Compared to **3** in 1:1 DMSO/H_2O, the deazaflavin did not achieve full conversion of **5** (85%) after 15 min. This could be explained by altered excited state energies and dynamics in this solvent system, evidenced by a bathochromic shift of the λ_{max} of **4** compared to PBS (from 389 to 395 nm, **Fig. 1b-c** and **Supplementary Fig. S1b**). Other flavin-derived photocatalysts such as deazaflavin **S1**[44] and alloxazine **S2**[45,46] (**Supplementary Figs. S1b** and **S3**) provided lower conversions of **5** (< 50%) most likely due to lower excited triplet energies. We therefore decided deazaflavin **4** was the optimal organic photocatalyst for diazirine activation, having superior activity over all other catalysts in PBS and can be readily prepared in two synthetic steps.

In addition to diazirines, we also screened our panel of photocatalysts for aryl azide (**S3**) conversion (E_T ≥ 43.8 kcal/mol),[9–11,25] resulting in 100% conversion for deazaflavin **4** and >75% for most others (**Supplementary Fig. S3**). However, control experiments without any photocatalyst showed blue light induced photolysis of aryl azide **S3** which has previously been reported.[11] On the other hand, the diazirine activation is purely dependent on the presence of **4** and blue light (**Fig. 1a** and **Supplementary Fig. S4**, entry 2) and can be achieved even in 5 min (**Supplementary Fig. S4** entry 3). Substitution of **4** at the *N*-3 position had no effect on its catalytic activity (**Supplementary Fig. S4**, entry 4), hence demonstrating this to be a useful site for attachment to a targeting modality for PPL application using DarT. Additionally, other diazirine probes containing amine and biotin handles can be activated using **4** (**Supplementary Fig. S4**, entries 5 and 6) and diazirine activation is possible in the presence of 10 mM GSH, albeit with reduced efficacy (55%, **Supplementary Fig. S4**, entry 7), to resemble intracellular PPL conditions.

Mechanistic validation of deazaflavin energy transfer

We then investigated the energy transfer mechanism of deazaflavin **4**, by first by performing a steady-state fluorescence quenching experiment and comparing aryl azide **6** to diazirine **7** (**Fig. 1d** and **Supplementary Fig. S5**).[19] A linear quenching relationship between deazaflavin **4** and **6** was observed with a rate constant (k_q) of 2.9×10^6 $M^{-1}s^{-1}$ determined from Stern-Volmer analysis, indicating **4** interacts with aryl azides in both singlet and triplet regimes (**Fig. 1d**). In contrast, non-linear fluorescence enhancement was observed using diazirine **7** indicating that **4** activates aryl diazirines exclusively *via* triplet energy transfer.[47,48] Given the lack of spectral overlap between the emission of **4** and probe absorption (**Fig. 1e** and **Supplementary Fig. S1c**), we can assume that a Dexter energy transfer mechanism is in place (**Fig. 1f**).[19]

We further explored the energy transfer capability of **4** using an intermediate trapping experiment with a model amine (*n*$BuNH_2$) and aryl azide **S4** (**Supplementary Fig. S6**).[9,11,25] In the excited state, aryl azides are known to rearrange into ketenimine intermediates that can undergo nucleophilic attack.[49] We therefore analysed the product distribution *via* ^{1}H NMR after irradiation of **S4** in the presence of **4** or iridium catalyst **3** as a control (10 mol%), and after blue LED (450 nm) or UV LED (365 nm) alone. Using deazaflavin **4** we observed the formation of reduced aniline **S5** (38%) and ketenimine **S6** (21%) as major products, indicating **4** is indeed capable of energy transfer to aryl azides. In the presence of iridium sensitiser **3** we observed the formation of azo compound **S7** (14%) and aniline **S5** (13%) without the formation of ketenimine **S6**, agreeing with previous findings.[9] When compared to light irradiation alone, 450 nm irradiation solely provides ketenimine **S6** (45%) and the starting material **S4** (44%) that concurs with other observations of aryl azide blue light reactivity.[11] 365 nm irradiation gives the expected ketenimine **S6** (32%) and aniline **S5** (8%). The sensitivity of aryl azides to blue light irradiation, despite having little to no spectral overlap (**Supplementary Fig. S1d**) is therefore a major limitation for their use in PPL experiments and are more suitable for green or red light dependant systems.[10,11,25]

Protein photolabelling

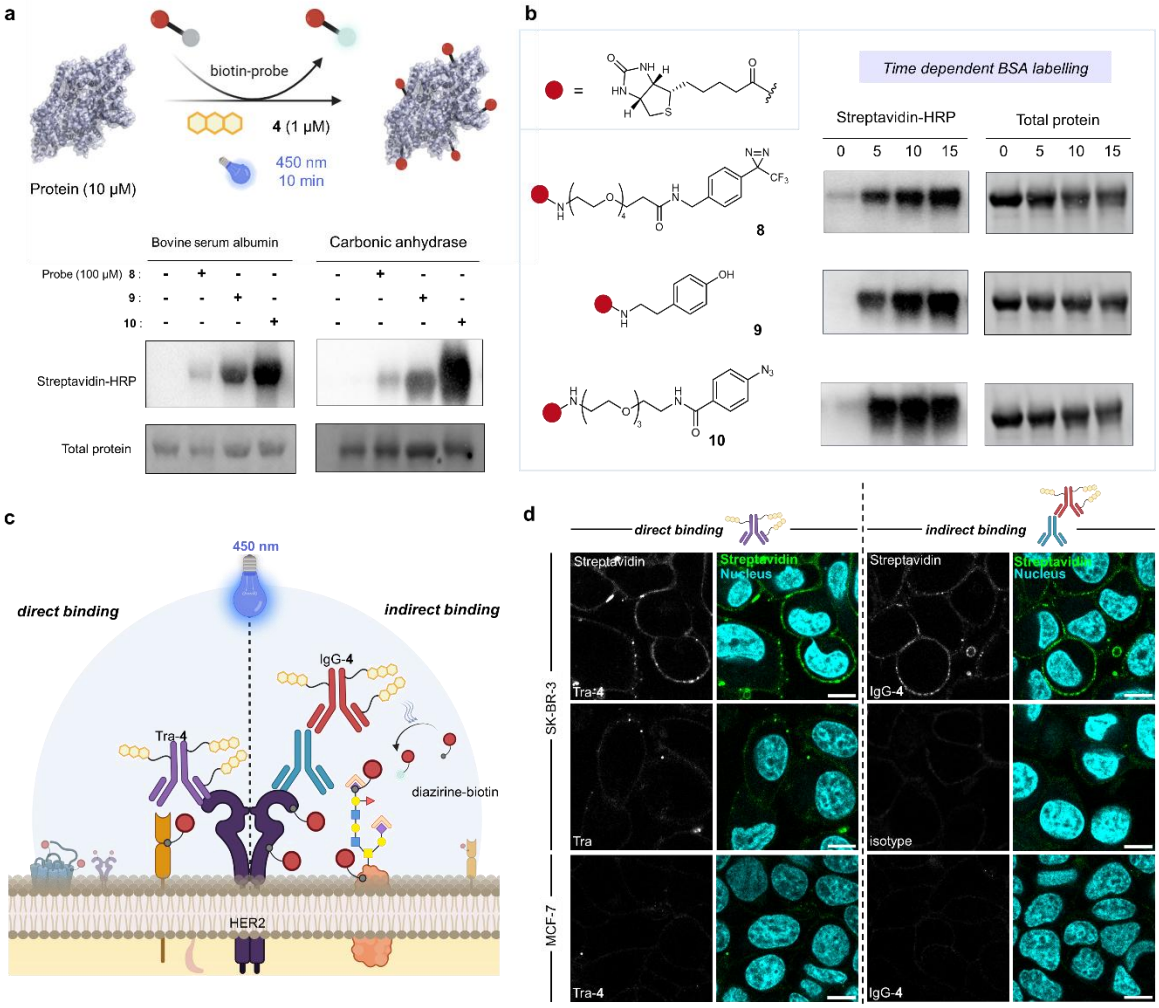

Fig. 2: Protein photolabelling *via* DarT on model proteins and cell surfaces using deazaflavin-antibody conjugates. a) Protein photolabelling using deazaflavin **4** (1 μM) in PBS pH 7.4 using various biotin-conjugated probes **8**-**10** (100 μM), PDB ID: 4F5S. **b)** Time dependant photolabelling of BSA (10 μM) using biotin probes **8**-**10** (100 μM) and deazaflavin **4** (1 μM) in PBS pH 7.4. **c)** Schematic presentation of cell surface labelling *via* DarT using HER2-targeted labelling employing either primary antibody-flavin conjugate Tra-**4** or secondary IgG-**4** in a direct and indirect approach, respectively. **d)** Confocal images of SK-BR-3 (HER2-positive) and MCF-7 (HER2-negative) cells treated with directly binding Tra-**4** or unmodified Trastuzumab as a control (left); or with the indirect primary/secondary system by using anti-HER2 antibody and IgG-**4** or a non-targeting isotype control (right). All conditions include subsequent incubation with 250 μM diazirine-biotin **8**, followed by blue LED irradiation for 10 min. Cells were additionally imaged for nuclei (Hoechst stain, blue); scale bars 10 μm.

We next sought to validate the capability of deazaflavin **4** to label model proteins using biotin-diazirine probe **8** (**Fig. 2a**) and additionally examine phenol **9** and aryl azide **10** to determine the suitability of deazaflavin **4** to multiscale PPL.[50] We anticipated the ability of deazaflavin **4** to activate phenol-based probes such as **9**, due to favourable electron transfer from the tyramide probe ($Tyr/Tyr^{\bullet+}$ = 1.08 vs. SCE)[22] to excited **4** (**4***/$\mathbf{4}^{\bullet-}$ ~ 1.20 V vs. SCE)[46] akin to their flavin relatives that have been previously utilised in PPL.[18,20–22] Effective protein biotinylation was

observed *via* Western blot for both bovine serum albumin (BSA) and carbonic anhydrase after 10 min blue LED irradiation for all three probes in the presence of **4** (10 mol%) (**Fig. 2a**). The diazirine probe shows comparably less intense bands compare to phenol or aryl azide probes due to their relative reactive half-lives, residue selectivity and photolysis of aryl azides. Importantly, protein labelling proved to be light and time dependent for all probes (**Fig. 2b**).

Taken together, these data show deazaflavin **4** is capable of multiscale PPL that has been shown to provide variable resolution in interactome profiling.[50] However, given the discussed limitations of aryl azide probe photolysis with blue light, and the lower oxidation potential of deazaflavins compared to its parent flavins (1.67 V vs. SCE for riboflavin tetraacetate),[20–22,51] we decided that diazirines are most suitable probe for deazaflavin-based PPL, thereby taking advantage of its distinctive energy transfer capability. This approach is henceforth termed DarT-labelling (deazaflavin-diazirine energy transfer labelling).

To validate DarT-labelling in a biological system, we chose a targeted PPL approach towards the cell surface receptor HER2, a membrane-bound receptor protein that is often overexpressed in breast cancer (**Fig. 2c**).[52] Cell surface PPL has progressed immensely in recent years and has revealed various novel interaction networks on and between the cell surfaces.[11,19,20,50,53] For extracellular target specificity we explored two different HER2 targeting antibody-based systems, the first being a deazaflavin-conjugate of the therapeutic antibody Trastuzumab (Tra-**4**) that was achieved through cysteine selective conjugation of **4** *via* an ethynyl-triazolyl-phosphinate (ETP) derivative.[54] The second approach consisted of a polyclonal anti-mouse IgG-**4** conjugate, facilitated through non-selective lysine modification.

DarT-labelling experiments were performed by treating HER2-overexpressing SK-BR-3 cells with either deazaflavin-antibody conjugate Tra-**4** or primary HER2-targeting antibody and subsequent treatment with IgG-**4** (**Fig. 2d**). After antibody treatment, diazirine-biotin probe **8** was added and carbene generation was triggered by 10 min blue LED (450 nm) irradiation. Cell surface biotinylation was visualised through confocal microscopy imaging using a Streptavidin-Alexa Fluor™ 488 conjugate that revealed clear fluorescent signal for Tra-**4** and IgG-**4** treated cells (**Fig. 2d**). Control experiments with unmodified Trastuzumab (Tra), an isotype primary IgG and HER2 negative cell line MCF-7 provided clear evidence of targeted extracellular DarT-labelling (**Fig. 2d**). Collectively, these data demonstrate the efficiency of DarT-labelling in complex extracellular environment and its versatility towards antibody-based PPL given both direct (Tra-**4**) to indirect (IgG-**4**) approaches provide efficient cell surface labelling.

Deazaflavin biocompatibility and cell permeability

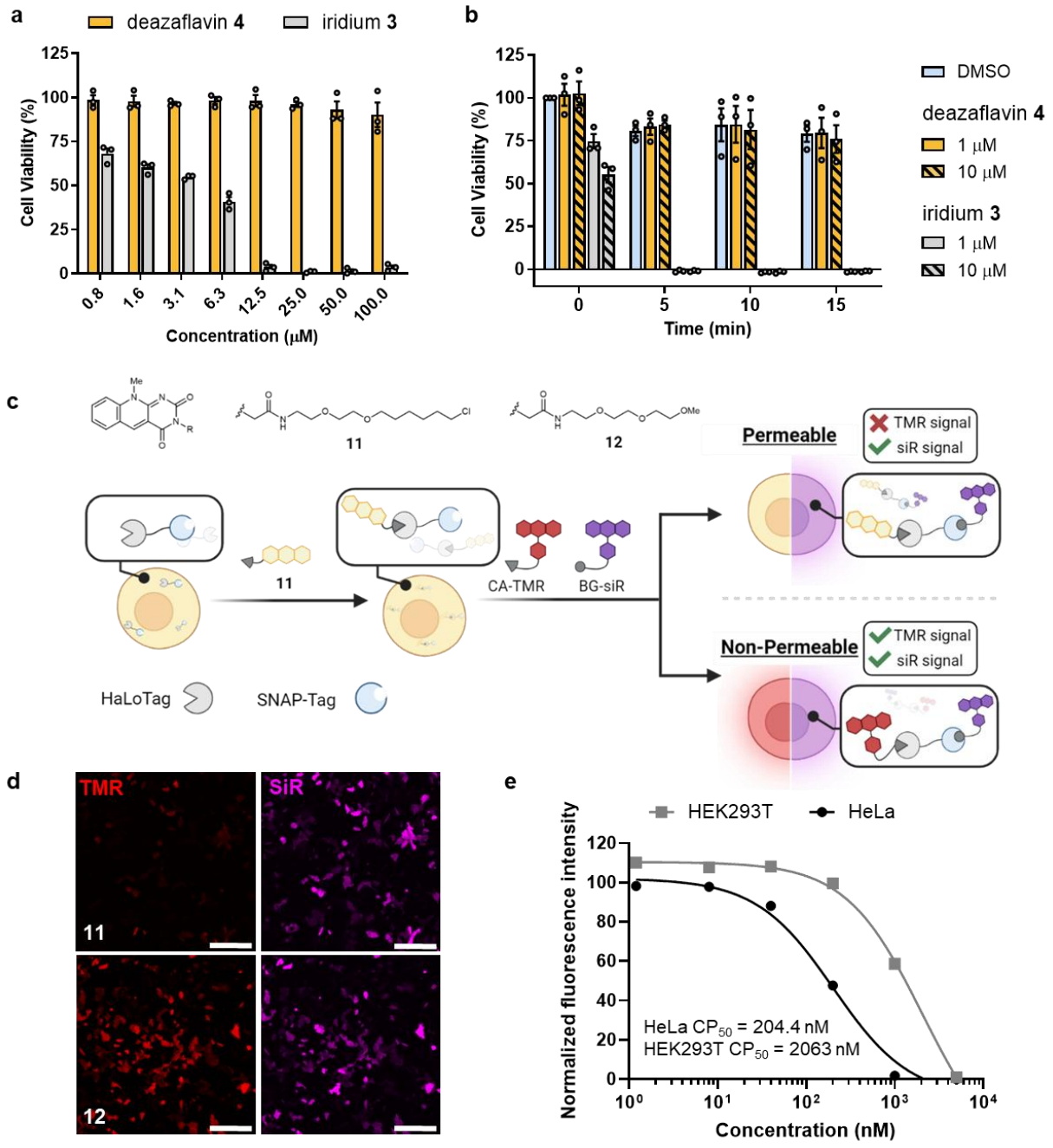

Fig. 3: Cellular biocompatibility and permeability of deazaflavin 4. a) Cytotoxicity assay (WST-1) of iridium **3** and deazaflavin **4** after 24 h incubation in HeLa cells. Data presented as mean ± standard error of mean (SEM) of three biological replicates. **b)** Light-induced toxicity of **3** and **4**. measured in HeLa cells after 24 h incubation following 450 nm irradiation (0-15 min) with pre-incubated catalysts (30 min). Data presented as mean ± SEM of three biological replicates. **c)** Scheme of chloroalkane penetration assay (CAPA) utilising chloroalkane-deazaflavin **11** and **12** as the negative control. Permeability is validated by CA-TMR-d12 and BG-SiR-d12 treatment. **d)** Tile-scan confocal microscopy of modified CAPA reporter HeLa cells treated with **11** or **12**, followed by CA-TMR-d12 and BG-SiR-d12. Scale bar = 100 μm. **e)** Normalised fluorescence intensity (TMR) of HeLa or HEK293T reporter cells following treatment of **11** at decreasing concentrations determined by flow cytometry. CP_{50} values for each reporter cell line is provided.

Prior to any intracellular application of DarT-labelling, we first validated the biocompatibility of deazaflavin **4** in live cells. Initially, the cytotoxicity of **4** was investigated in comparison to the well-established iridium photocatalyst **3**. HeLa cells were incubated for 24 h in the presence of varying concentrations of **4** and **3** and the resulting viability was measured *via* WST-1 assay (**Fig. 3a**). The data reveals a considerable cytotoxic effect of iridium catalyst **3** when compared to **4**, evidenced by as little as 0.78 µM **3** reducing viability to <70%, which is in contrast to a previous report using the same catalyst,[35] but recent data aligns with our findings.[33] However, even at a very high concentration (100 µM), cells maintained a viability of >85% in the presence of **4**, confirming its excellent biocompatibility.

We further investigated phototoxicity of **3** and **4** by irradiating HeLa cells with 450 nm light for 0 to 15 min after pre-incubating the catalysts for 1 h and measuring viability using the WST assay after 24 h incubation (**Fig. 3b**). Even after 5 min of irradiation, iridium **3** completely reduces cell viability to 0% at both 1 and 10 µM. On the other hand, cells treated with deazaflavin **4** and irradiated for 5 min demonstrated very low phototoxicity (>80% viability at 1 and 10 µM) which is comparable to the DMSO control. Blue light irradiation alone is known to induce oxidative stress by excitation of endogenous photosensitisers that is evidenced by our data through reducing cell viability to 79% after 15 min irradiation.[55] Deazaflavin **4** therefore has little additional phototoxic effect to the cells after this irradiation time as cell viability is reduced to 76% with 10 µM treatment of **4**. Compared to iridium complexes[56] and other flavin derivatives, deazaflavins are known to be the least singlet oxygen sensitising (ϕ_Δ = 0.33 for 5-deazariboflavin),[57] which could therefore explain these observations.

Cell permeability of deazaflavin **4** was confirmed using a modified pulse-chase chloroalkane penetration assay (CAPA) in HeLa and HEK cell lines (**Fig. 3c**).[58] We first conjugated a chloroalkane (CA) linker to the *N*-3 positon of the scaffold to give deazaflavin-chloroalkane **11** that was used to pulse reporter cells expressing cytoplasmic HaloTag-SNAP-tag fusion protein. Cells were first treated with **11** in order to covalently label the active site of the HaloTag (if cell permeable) and excess non-internalised molecules were washed away. Subsequent treatment with cell-permeable red CA-TMR-d12 and far-red BG-SiR-d12[59] treatment results in CA-TMR-d12 reacting with the remaining unoccupied HaloTag, while BG-SiR-d12 is used to occupy the SNAP-tag that is employed as an expression control to normalise for transient transfection (**Fig. 3c**). Confocal microscopy images confirm that the treatment of **11** resulted to fewer unoccupied HaloTag, hence lower TMR signal, whereas treatment with non-reactive triethylene glycol derivative **12** showed no decrease in TMR signal (**Fig. 3d**). We quantified the CP_{50} (treatment

concentration where 50% of the expressed HaloTags are labelled) by titrating the treatment concentrations of **11** and measuring the mean fluorescence intensities (MFI) of the reporter cells by flow cytometry. We show evidence that **11** is cell-permeable in both HeLa and HEK293T reporter cells with CP_{50} of 204.4 nM and 2063 nM, respectively (**Fig. 3e**). The discrepancy in CP_{50} values indicates variable degree of penetration propensity of the deazaflavin with different cell lines, which may be due to the overall physiology of the specific cell line in question. Overall, the excellent biocompatibility and cell-permeability of deazaflavin **4** positions DarT-labelling as a highly suitable methodology for intracellular PPL applications.

Intracellular mapping of R_{10} peptide interactomes via DarT-labelling

From its initial discovery, cell-penetrating peptides (CPPs) have been a popular strategy utilised by various groups to deliver a myriad of extracellular cargoes into cells.[60] Our group in particular has employed polyarginine CPPs for a number of intracellular delivery applications of various functional proteins.[61–63] Despite its broad application and popularity among the intracellular delivery community, questions still remain regarding their mechanism of action, intracellular interacting partners, and influence on overall cellular physiology. Futaki and coworkers have previously applied diazirine-based photocrosslinking using UV light to identify intracellular and extracellular interactors of R_8.[64,65] Due to the inefficiency of diazirine photocrosslinking chemistry,[66] this assay requires exceptionally large amount of treated cells, whilst providing very few reliable hits. We questioned whether we could utilise deazaflavin **4** and diazirine **8** to label the intracellular protein binders of each of our widely used linear and cyclic decaarginines (R_{10}) *via* photocatalytic energy transfer (**Fig. 4a**), which would otherwise not be possible with cytotoxic iridium PCs.[34] This could help to provide a better understanding the intracellular fate of Arg-rich CPPs and as a result, the development of future intracellular delivery and targeting applications.

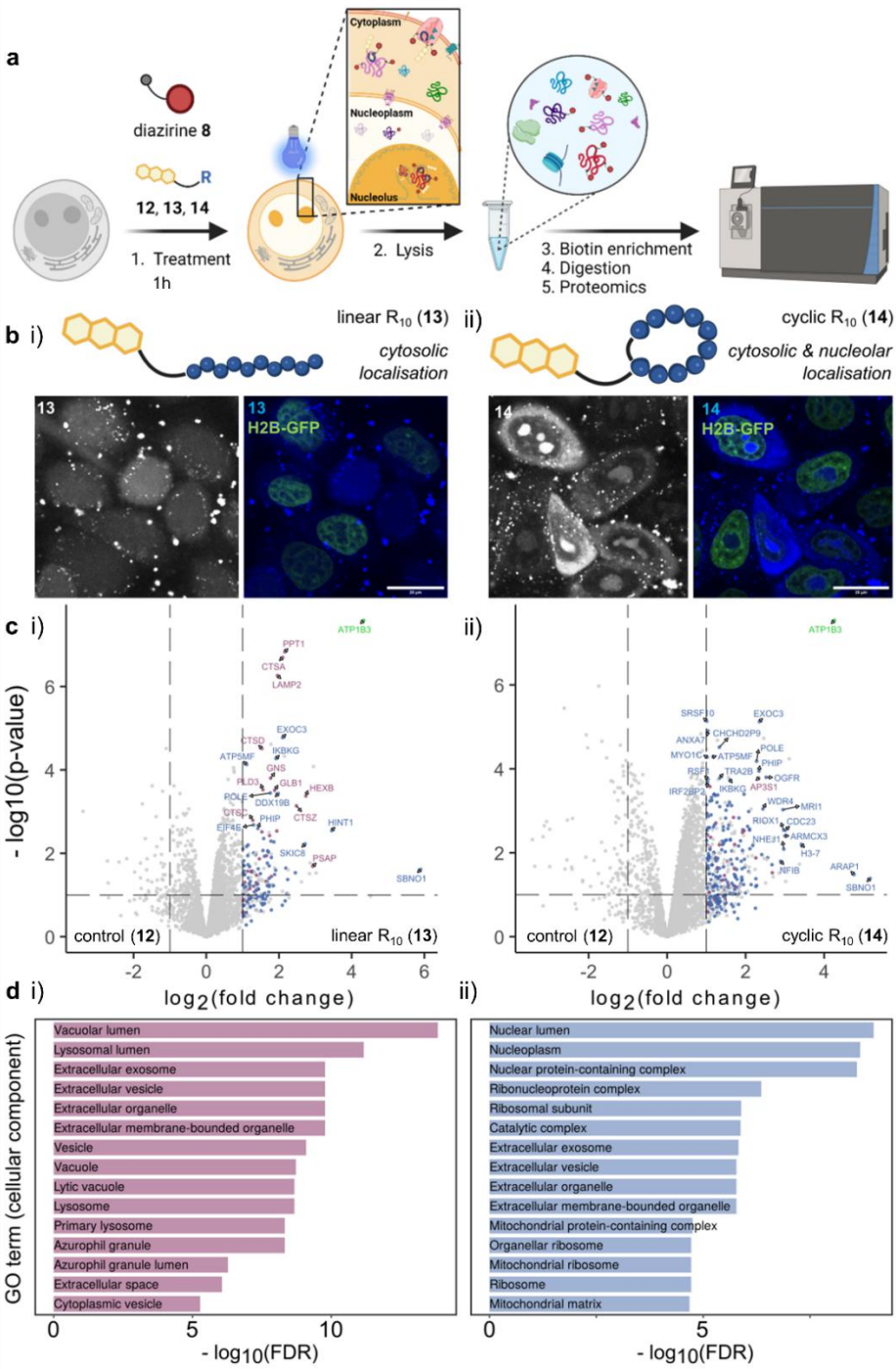

Fig. 4: Mapping CPP interactomes *via* DarT-labelling. a) Intracellular DarT-labelling workflow for polyarginine CPP interactome mapping. **b)** Confocal microscopy images of HeLa cells stably expressing histone 2B-green fluorescent protein (H2B-GFP) fusion protein treated with **i)** linear R_{10}-deazaflavin conjugate **13** (20 µM) and **ii)** cyclic R_{10}-deazaflavin conjugate **14** (20 µM). Scale bars: 20 µm. **c)** Volcano plots from label-free quantification (LFQ) analysis of HeLa cells treated with **i)** linear R_{10} conjugate **13** vs deazaflavin conjugate **12** (5 µM) and **ii)** cyclic R_{10} conjugate **14** vs deazaflavin conjugate **12** (5 µM) for 1 h using diazirine **8** (250 µM) and 15 min irradiation (450 nm). Significantly enriched proteins (p-value < 0.05 and $\log_2$FC > 1) are coloured with the most significantly enriched proteins from gene ontology (GO) term 'cellular compartment' labelled relating to lysosome (purple), nucleus (blue) and membrane ion channel (green). **d)** GO analysis of significantly enriched proteins relating to 'cellular compartment' for **i)** linear R_{10} conjugate **13** vs deazaflavin conjugate **12** and **ii)** cyclic R_{10} conjugate **14** vs deazaflavin conjugate **12** data sets.

We first attached deazaflavin **4** to the *N*-terminus of each CPP and treated HeLa cells with the resulting deazaflavin-CPP conjugates (linear **13** and cyclic **14**, 20 μM) for 1 h. Thanks to the inherent fluorescence of the deazaflavin moiety (λ_{em} = 450 nm, **Fig. 1b**), the cells could be imaged to verify successful delivery of the peptides. Linear R_{10} peptides generally localise in the cytosol and can be entrapped in endosomes when administered to cells.[67] On the other hand, cyclic R_{10} variants are more efficient and robust CPP derivatives that enters via direct translocation into cells and are capable of nucleolar localisation.[67] Confocal microscopy confirmed effective delivery and anticipated localisation patterns of deazaflavin-CPP conjugates in which linear derivative **13** was observed in the cytosol and cyclic **14** showed clear nucleolar localisation as well as cytosolic (**Fig. 4b**). To validate intracellular DarT-labelling, cells were incubated with **13**, **14** or control deazaflavin **12** (20 μM) for 1 h, subsequently washed and treated with diazirine **8** (30 min, 250 μM) before irradiating with 450 nm for 15 min. Western blot analysis of fractionated lysates revealed successful intracellular labelling and a clear trend in biotinylated proteins (**Supplementary Fig. S7**). As expected, cyclic **14** elicits the highest degree of labelling across all fractions, especially within nuclear extracts when compared to linear **13** and control **12**. This correlated well to microscopy imaging and encouraged us to perform further enrichment and label-free quantification (LFQ) proteomic analysis to identify the R_{10} peptides' interactome (**Fig. 4a**).

We therefore repeated the intracellular DarT-labelling experiment for LFQ proteomic analysis after 1 h incubation of deazaflavin-CPPs at 5 μM in order to reduce potential background labelling and peptide aggregation. To help resolve R_{10}-specific protein interactors, we use unconjugated deazaflavin **12** as the control. Following diazirine incubation (30 min, 250 μM), irradiation (15 min, 450 nm) and biotin enrichment using magnetic streptavidin beads, biotinylated proteins were digested and subjected to LC-MS/MS analysis. LFQ analysis obtained volcano plots that revealed a large number of significantly enriched proteins ($\log_2$ fold change >2.0) for both deazaflavin-CPP conjugates. As anticipated, linear R_{10} conjugate **13** displays a number of significantly enriched lysosomal proteins such as lysosomal protective proteins, cathepsin A and D (CTSA and CTSD), lysosome-associated membrane glycoprotein 2 (LAMP2) and palmitoyl-protein thioesterase 1 (PPT1) (**Fig. 4c, i**). On the other hand, cyclic R_{10} **14** featured more proteins associated to the nucleus and nucleolus such as strawberry notch homolog 1 (SBNO1), histone H3-7, PH domain-binding protein (PHIP) and WD repeat domain 4 (WDR4) (**Fig. 4c, ii**).

By performing gene ontology (GO) enrichment analysis we were able to identify trends in the enriched proteins to cellular compartments that align with their expected subcellular localisation (**Fig. 4d**). For example, linear R_{10} conjugate **13** displayed a high degree of endosomal and

lysosomal enrichment (**Fig. 4d, i**), whereas cyclic **14** featured a greater number of nuclear and nucleolus-associated proteins (**Fig. 4d, ii**). A Venn diagram comparing significantly enriched proteins from both CPPs revealed >3 times the number of unique proteins associated to the cyclic R_{10} compared to linear R_{10} (**Supplementary Fig. S8a**). This can be rationalised by the greater uptake efficacy of the cyclic derivative and prominent nucleolar localisation, evidenced by its unique GO terms for nuclear and ribosomal proteins (**Supplementary Fig. S8b**). Due to both CPPs displaying cytosolic localisation, we observed a large number of shared significantly enriched proteins (around 27%) that relate to lysosomal and granule-associated proteins (**Supplementary Fig. S8c** and **d**). Altogether, this demonstrates DarT-labelling can enable the unbiased proteomic identification of proteins interacting with R_{10} CPPs across multiple subcellular compartments, such as the lysosome and nucleolus, that aligns with expected patterns from confocal microscopy.

We also observed the significant enrichment of some cell membrane proteins that could be involved in the uptake of the R_{10} CPPs. Previously, the Futaki lab identified R_8 CPP protein interactors such as the intracellular LanCL1[64] and extracellular syndecan-4, a receptor for clathrin-mediated endocytosis of the CPPs using UV light activation of aryl diazirines.[65] However, we were not able to identify these proteins in our proteomic data, most likely due to different incubation conditions of the CPPs with the cells (4 ^{o}C for 0.5 to 5 min).[64,65] However, one significantly enriched protein common to both linear and cyclic R_{10} data sets ($\log_2$ fold change >4.0, p-value < 0.001) that caught our attention was the ATPase Na^+/K^+ transporting subunit beta 3 (ATP1B3, **Fig. 4c**). As an integral membrane protein, ATP1B3 is responsible for establishing and maintaining the electrochemical Na^+/K^+ gradient across the plasma membrane and is ranked within the top 25% of abundant proteins within the cell line employed (HeLa, **Supplementary Fig. S9**).[68] These gradients are fundamental for osmoregulation and the sodium-coupled transport of various organic and inorganic solutes.[69] Interestingly, the Widmann group has recently identified ATP1B3 as a key regulator of TAT CPP cellular uptake.[70] We therefore hypothesise that this ion pump is involved in regulating the uptake of R_{10} CPPs regardless of their structure and our future work aims to biologically validate these findings.

DarT-labelling in live cells after 24 h

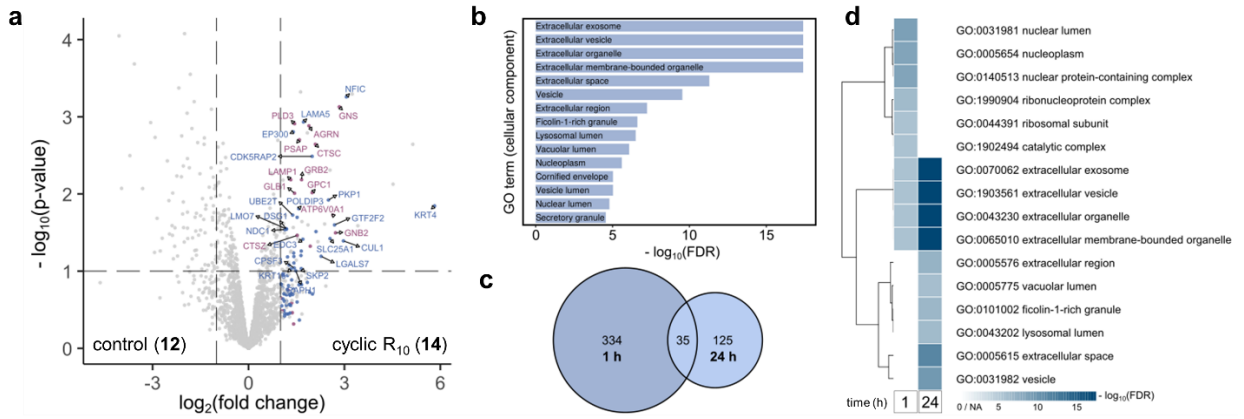

Fig. 5: Mapping the cyclic R_{10} interactome after 24 h. a) Volcano plot from label-free quantification (LFQ) analysis of HeLa cells treated with cyclic R_{10} **14** vs deazaflavin **12** (5 µM) 24 h post-treatment using diazirine **8** (250 µM) and 15 min irradiation (450 nm). Significantly enriched proteins (p-value < 0.05 and log_2FC > 1) are coloured with the most significantly enriched proteins from gene ontology (GO) term of 'cellular compartment' labelled relating to lysosome (purple) and nucleus (blue). **b)** GO terms (cellular compartment) of significantly enriched proteins relating to cyclic R_{10} **14** vs control **12** 24 h post-treatment. **c)** Venn diagram comparing significantly enriched proteins from DarT-labelling after 1 h incubation and 24 h post-treatment of cyclic R_{10} **14**. **d)** Clustered heatmap of GO terms relating to 'cellular compartment' after 1 h incubation and 24 h post-treatment of **14**.

Recognising the robust biocompatibility of deazaflavin **4** over other reported photocatalysts capable of diazirine activation,[34] we envisioned that DarT-labelling could be utilised for long-term incubation experiments to map dynamic intracellular events with high resolution. Our group, and others, have observed stark differences in the cellular clearance of linear and cyclic R_{10} peptides by confocal microscopy, in which the linear R_{10} peptide undergoes lysosomal degradation and peptidolysis (**Supplementary Fig. S10a**), whereas the cyclic derivative clearly remains present within the cell post-treatment and localises within intracellular vesicles with some nucleolar signal remaining (**Supplementary Fig. S10b**). This can be rationalised by its superior stability to peptidolysis due to its cyclic nature and incorporation of D-amino acids into the R_{10} sequence.[71] With this in mind, we questioned whether DarT-labelling remains applicable after 24 hour post-treatment of cells with cyclic R_{10} **14**, therefore highlighting its suitability to map transient or dynamic intracellular trafficking.[72,73]

We therefore treated cells with **14** for 1 h and subsequently exchanged for fresh media followed by a further 24 h incubation at 37 °C. Cells were then treated with diazirine-biotin **8** (250 µM, 30 min at 37 °C) and irradiated with 450 nm light for 15 min. Following lysis, biotin enrichment and LFQ analysis of the proteomic data, we obtained a volcano plot that revealed a number of enriched proteins found in exosomes and lysosomes, such as glucosamine (N-Acetyl)-6-Sulfatase (GNS), lysosome-associated membrane glycoprotein 1 (LAMP1), prosaposin (PSAP)

and cathepsin C (CTSC) (**Fig. 5a**). Interestingly, we only detected significant enrichment of intravesicular and transmembrane proteins associated with exosomes and lysosomes. Other typical intracellular vesicle markers, such as Rab proteins, were not significantly enriched (log_2 fold change <1.0). This implies the photocatalyst-peptide conjugate is entrapped within the vesicle and does not reside outside of membrane.

GO analysis of the enriched proteins in relation to their cellular compartment consolidates our findings, displaying a significant enrichment of exosome, granule and lysosome-associated proteins, as well as some nucleus-associated proteins (**Fig. 5b**). To further validate these findings, we utilised a TMR-conjugated cyclic R_{10} to observe changes in localisation after 24 h post-treatment (**Supplementary Fig. S10**), as the deazaflavin fluorescence was too weak to be reliably detected at lower concentrations. The images show the loss of nuclear and nucleolar fluorescent signals over time with pronounced localisation within endo/lysosomes, further indicating the peptide may undergo lysosomal exocytosis. Lysosomal exocytosis is a ubiquitous physiological phenomenon performed by cells to maintain cellular homeostasis, as well as to protect from accumulation of toxic products, such as heavy metals and aggregated proteins.[74]

To gain further evidence of this phenomenon, we compared the overall number of proteins enriched after 1 h incubation and 24 post-treatment (**Fig. 5c**). >2 times fewer proteins were enriched after 24 h, which could therefore be explained by lysosomal exocytosis of internalised cyclic R_{10} **14** over time. Lastly, comparing the enriched GO terms from 1 h incubation and 24 h post-treatment (**Supplementary Fig. S11**) and subsequently clustering the enrichment FDR (false discovery rate of adjusted P-value) of the terms, allowed us to better observe trafficking of the peptide (**Fig. 5d**). A clear decrease in nuclear and nucleolus-associated proteins is apparent, coupled by a vast increase in lysosomal and exocytosis-associated proteins. Cyclic R_{10} **14** is therefore not processed through a conventional degradation pathway due to peptidolysis stability, and is ultimately collected into lysosomes that are expelled from cells through an exocytosis pathway.

Taken together, we have demonstrated that DarT-labelling can be utilised to map the subcellular trafficking of a cyclic R_{10} peptide after prolonged incubation. Our data reflect that the peptide undergoes a prominent exocytosis mechanism most likely due to its stability against peptidases, which could translate to other cyclic and D-amino acid containing peptides. There are only few reports regarding the intracellular fate of such species and more knowledge concerning these factors could enhance their translation to biopharmaceutical applications.[75,76] More generally, the ability of DarT-labelling to be performed inside cells over time highlights its unprecedented

suitability to facilitate proximity labelling with precise spatiotemporal control to map dynamic cellular processes.[72,73]

Conclusions

In summary, we have discovered a readily accessible organic photocatalyst, deazaflavin **4**, that is capable of activating diazirine probes by energy transfer to enable the labelling of both extra- and intracellular proteins in live cells for precise microenvironment mapping (termed DarT-labelling).[19] We showed that **4** activates diazirine probes only *via* triplet energy transfer and can additionally be utilised in aryl azide and phenol-based protein labelling. Deazaflavin **4** exhibited excellent cell-permeability and biocompatibility as well as limited phototoxicity, especially when compared to the iridium photocatalyst **3**, which was key to using deazaflavin-conjugates for intracellular PPL upon extended incubations in live cells.

We demonstrated the prospect of intracellular DarT-labelling to probe the interactome of linear and cyclic arginine-containing CPPs across multiple subcellular compartments. LFQ proteomic analysis resulted in a number of significantly enriched proteins for both CPPs that correlated well to their expected localisation thanks to the intrinsic fluorescence of **4**. Further Gene Ontology (GO) enrichment revealed the classification of proteins by cellular compartment, confirming that endo- and lysosomal proteins were primarily targeted by linear CPPs whereas cyclic derivatives predominantly interacted with nucleolar proteins. Within this workflow, we were able to identify the interaction of both CPPs with the integral Na^+/K^+ ion channel ATP1B3, which has previously been proposed to regulate TAT peptide uptake into cells,[70] suggesting that this ion channel is more generally associated to arginine-rich CPPs-uptake mechanisms..

Finally, we investigated the intracellular fate of the cyclic R_{10} derivative, which supports the use of DarT-labelling to map live cell trafficking after extended time points. After 24 h post-treatment of the cyclic CPP, we primarily enriched proteins related to exosomes, granules and lysosomes that points towards the potential excretion pathway of the undigested cyclic R_{10} from the cell. This further highlights the excellent biocompatibility of deazaflavin **4** and its ability to be utilised for diazirine-based intracellular PPL with unique spatiotemporal control. Overall, DarT-labelling offers a powerful, dynamic and precise method for interactome mapping to aid our understanding of essential intracellular mechanisms and elucidate complex disease-related biomolecular networks.

Acknowledgements

We wish to thank Ramona Birke, Kilian Roßmann and Dr. Johannes Broichagen (J.B.) for supplying HaloTag and SNAP-tag reagents (CA-NHBoc, CA-TMR-d12 and BG-SiR-d12) and plasmid (pcDNA5_FRTcyto_Halo-SNAP-meGFP) for the modified CAPA. We thank Heike Stephanowitz, Ines Kretzschmar and Beate Kindt for their technical assistance and J.B. for helpful discussions. We thank Dr. Mark A. R. de Geus for his technical assistance for the synthesis and conjugation of Tra-**4**. J.V.V.A. was funded by an Alexander von Humboldt Fellowship. C.P.R.H. acknowledges support from the Deutsche Forschungsgemeinschaft (DFG, RTG2473 “Bioactive Peptides” Projektnummer 392923329 and CRC 1449 Projektnummer 431232613).

Author Contributions

L.B.C., J.M.M., J.V.V.A., C.E.S. and C.P.R.H. conceived the work. L.B.C. and J.M.M. designed, synthesised and executed photocatalyst screening and protein labelling. J.M.M. performed extracellular labelling experiments. K.K.H. performed cell cytotoxicity experiments. K.R. synthesised all HaloTag and SNAP-tag reagents used for the CAPA assay and J.V.V.A. performed the assay. J.V.V.A carried out all cellular imaging for CAPA and CPP localisation. L.B.C. and J.V.V.A. prepared the samples and performed the CPP interactome mapping experiments. M.R. performed proteomic-based data analysis and output. L.B.C., J.M.M., J.V.V.A., F.L. and M.R. interpreted proteomic-based experiments. L.B.C., J.V.V.A., J.M.M. and C.P.R.H. wrote the manuscript, with input from all authors.

References

1. Chen, L., Wang, R. S. & Zhang, X. S. *Biomolecular Networks: Methods and Applications in Systems Biology*. (John Wiley and Sons, 2009). doi:10.1002/9780470488065.

2. Bludau, I. & Aebersold, R. Proteomic and interactomic insights into the molecular basis of cell functional diversity. *Nat. Rev. Mol. Cell Biol.* **21**, 327–340 (2020).

3. Kang, M. G. & Rhee, H. W. Molecular Spatiomics by Proximity Labeling. *Acc. Chem. Res.* **55**, 1411–1422 (2022).

4. Keskin, O., Tuncbag, N. & Gursoy, A. Predicting Protein-Protein Interactions from the Molecular to the Proteome Level. *Chem. Rev.* **116**, 4884–4909 (2016).

5. Luck, K. *et al.* A reference map of the human binary protein interactome. *Nat. 2020 5807803* **580**, 402–408 (2020).

6. Bosch, J. A., Chen, C. L. & Perrimon, N. Proximity-dependent labeling methods for proteomic profiling in living cells: An update. *Wiley Interdiscip. Rev. Dev. Biol.* **10**, e392 (2020).

7. Fang, Y. & Zou, P. Photocatalytic Proximity Labeling for Profiling the Subcellular Organization of Biomolecules. *ChemBioChem* **24**, e202200745 (2023).

8. Knutson, S. D., Buksh, B. F., Huth, S. W., Morgan, D. C. & MacMillan, D. W. C. Current advances in photocatalytic proximity labeling. *Cell Chem. Biol.* **31**, 1145–1161 (2024).

9. Oakley, J. V. *et al.* Radius measurement via super-resolution microscopy enables the development of a variable radii proximity labeling platform. *Proc. Natl. Acad. Sci. U. S. A.* **119**, 1–8 (2022).

10. Buksh, B. F. *et al.* μmap-Red: Proximity Labeling by Red Light Photocatalysis. *J. Am. Chem. Soc.* **144**, 6154–6162 (2022).

11. Tay, N. E. S. *et al.* Targeted activation in localized protein environments via deep red photoredox catalysis. *Nat. Chem.* **15**, 101–109 (2023).

12. Ryu, K. A. *et al.* Near-Infrared Photoredox Catalyzed Fluoroalkylation Strategy for Protein Labeling in Complex Tissue Environments. *ACS Catal.* 3482–3491 (2024) doi:10.1021/ACSCATAL.4C00447.

13. Takato, M. *et al.* Photoproximity labeling of endogenous receptors in the live mouse brain in minutes. *Nat. Chem. Biol.* (2024) doi:10.1038/s41589-024-01692-4.

14. Shu, X. *et al.* A genetically encoded tag for correlated light and electron microscopy of intact cells, tissues, and organisms. *PLoS Biol.* **9**, e1001041 (2011).

15. To, T. L. *et al.* Photoactivatable protein labeling by singlet oxygen mediated reactions. *Bioorganic Med. Chem. Lett.* **26**, 3359–3363 (2016).

16. Zhai, Y. *et al.* Spatiotemporal-resolved protein networks profiling with photoactivation dependent proximity labeling. *Nat. Commun.* **13**, 1–12 (2022).

17. Zheng, F., Yu, C., Zhou, X., Zou, P. & Yu, C. Genetically encoded photocatalytic protein labeling enables spatially-resolved profiling of intracellular proteome. *Nat. Commun.* **14**, 1–14 (2023).

18. Hananya, N., Ye, X., Koren, S. & Muir, T. W. A genetically encoded photoproximity labeling

approach for mapping protein territories. *Proc. Natl. Acad. Sci. U. S. A.* **120**, (2023).

19. Geri, J. B. *et al.* Microenvironment mapping via Dexter energy transfer on immune cells. *Science (80-.).* **367**, 1091–1097 (2020).

20. Oslund, R. C. *et al.* Detection of cell–cell interactions via photocatalytic cell tagging. *Nat. Chem. Biol.* **18**, 850–858 (2022).

21. Bechtel, T. J. *et al.* Proteomic mapping of intercellular synaptic environments via flavin-dependent photoredox catalysis. *Org. Biomol. Chem.* **21**, 98–106 (2022).

22. Hope, T. O. *et al.* Targeted proximity-labelling of protein tyrosines via flavin-dependent photoredox catalysis with mechanistic evidence for a radical–radical recombination pathway . *Chem. Sci.* **14**, 7327–7333 (2023).

23. Tamura, T., Takato, M., Shiono, K. & Hamachi, I. Development of a photoactivatable proximity labeling method for the identification of nuclear proteins. *Chem. Lett.* **49**, 145–148 (2020).

24. Tsushima, M. *et al.* Intracellular photocatalytic-proximity labeling for profiling protein-protein interactions in microenvironments. *Chem. Commun.* **58**, 1926–1929 (2022).

25. Wang, H. *et al.* Selective Mitochondrial Protein Labeling Enabled by Biocompatible Photocatalytic Reactions inside Live Cells. *JACS Au* **1**, 1066–1075 (2021).

26. Wang, H. *et al.* A photo-oxidation driven proximity labeling strategy enables profiling of mitochondrial proteome dynamics in living cells. *Chem. Sci.* **13**, 11943–11950 (2022).

27. Zhai, Y. *et al.* Global profiling of functional histidines in live cells using small-molecule photosensitizer and chemical probe relay labelling. *Nat. Chem.* **16**, 1546–1557 (2024).

28. Folkes, L. K., Trujillo, M., Bartesaghi, S., Radi, R. & Wardman, P. Kinetics of reduction of tyrosine phenoxyl radicals by glutathione. *Arch. Biochem. Biophys.* **506**, 242–249 (2011).

29. Rizk, M. S., Shi, X. & Platz, M. S. Lifetimes and reactivities of some 1,2-didehydroazepines commonly used in photoaffinity labeling experiments in aqueous solutions. *Biochemistry* **45**, 543–551 (2006).

30. Gorman, A. A. & Rodgers, M. A. J. New trends in photobiology: Current perspectives of singlet oxygen detection in biological environments. *J. Photochem. Photobiol. B Biol.* **14**, 159–176 (1992).

31. Skovsen, E., Snyder, J. W., Lambert, J. D. C. & Ogilby, P. R. Lifetime and diffusion of singlet oxygen in a cell. *J. Phys. Chem. B* **109**, 8570–8573 (2005).

32. Trowbridge, A. D. *et al.* Small molecule photocatalysis enables drug target identification via energy transfer. *Proc. Natl. Acad. Sci. U. S. A.* **119**, 1–8 (2022).

33. Pan, C., Knutson, S. D., Huth, S. W. & MacMillan, D. W. C. µMap proximity labeling in living cells reveals stress granule disassembly mechanisms. *Nat. Chem. Biol.* (2024) doi:10.1038/s41589-024-01721-2.

34. Dolan, C. *et al.* Cell uptake and cytotoxicity of a novel cyclometalated iridium(III) complex and its octaarginine peptide conjugate. *J. Inorg. Biochem.* **119**, 65–74 (2013).

35. Huang, Z. *et al.* Bioorthogonal Photocatalytic Decaging-Enabled Mitochondrial Proteomics. *J. Am. Chem. Soc.* **143**, 18714–18720 (2021).

36. Liu, Z. *et al.* Bioorthogonal photocatalytic proximity labeling in primary living samples. *Nat. Commun. 2024 151* **15**, 1–18 (2024).

37. Walsh, C. Naturally Occurring 5-Deazaflavin Coenzymes: Biological Redox Roles. *Acc. Chem. Res.* **19**, 216–221 (1986).

38. Nikitas, N. F., Gkizis, P. L. & Kokotos, C. G. Thioxanthone: a powerful photocatalyst for organic reactions. *Org. Biomol. Chem.* **19**, 5237–5253 (2021).

39. Alonso, R. & Bach, T. A chiral thioxanthone as an organocatalyst for enantioselective [2+2] photocycloaddition reactions induced by visible light. *Angew. Chemie - Int. Ed.* **53**, 4368–4371 (2014).

40. Tröster, A., Alonso, R., Bauer, A. & Bach, T. Enantioselective Intermolecular [2 + 2] Photocycloaddition Reactions of 2(1H)-Quinolones Induced by Visible Light Irradiation. *J. Am. Chem. Soc.* **138**, 7808–7811 (2016).

41. Elliott, L. D., Kayal, S., George, M. W. & Booker-Milburn, K. Rational design of triplet sensitizers for the transfer of excited state photochemistry from UV to visible. *J. Am. Chem. Soc.* **142**, 14947–14956 (2020).

42. Irshadeen, I. M. *et al.* Action Plots in Action: In-Depth Insights into Photochemical Reactivity. *J. Am. Chem. Soc.* **143**, 21113–21126 (2021).

43. Bliese, M., Launikonis, A., Loder, J. W., Mau, W. H. A. & Sasse, W. H. F. Photoreduction

of deazaflavin. Spectroscopic investigations. *Aust. J. Chem.* **36**, 1873–1883 (1983).

44. Graml, A., Neveselý, T., Jan Kutta, R., Cibulka, R. & König, B. Deazaflavin reductive photocatalysis involves excited semiquinone radicals. *Nat. Commun.* **11**, 1–11 (2020).

45. Mojr, V. *et al.* Tailoring flavins for visible light photocatalysis: organocatalytic [2+2] cycloadditions mediated by a flavin derivative and visible light. *Chem. Commun.* **51**, 12036–12039 (2015).

46. Mojr, V. *et al.* Flavin Photocatalysts for Visible-Light [2+2] Cycloadditions: Structure, Reactivity and Reaction Mechanism. *ChemCatChem* **10**, 849–858 (2018).

47. Altman, R. B. *et al.* Cyanine fluorophore derivatives with enhanced photostability. *Nat. Methods* **9**, 68–71 (2012).

48. Gong, W. *et al.* Redefining the photo-stability of common fluorophores with triplet state quenchers: Mechanistic insights and recent updates. *Chem. Commun.* **55**, 8695–8704 (2019).

49. Inui, H., Sawada, K., Oishi, S., Ushida, K. & McMahon, R. J. Aryl nitrene rearrangements: Spectroscopic observation of a benzazirine and its ring expansion to a ketenimine by heavy-atom tunneling. *J. Am. Chem. Soc.* **135**, 10246–10249 (2013).

50. Lin, Z. *et al.* Multiscale photocatalytic proximity labeling reveals cell surface neighbors on and between cells. *Science* **385**, eadl5763 (2024).

51. Mühldorf, B. & Wolf, R. Photocatalytic benzylic C-H bond oxidation with a flavin scandium complex. *Chem. Commun.* **51**, 8425–8428 (2015).

52. Gutierrez, C. & Schiff, R. HER2 Biology, Detection, and Clinical Implications. *Arch. Pathol. Lab. Med.* **135**, 55–62 (2011).

53. Bartholow, T. G. *et al.* Photoproximity Labeling from Single Catalyst Sites Allows Calibration and Increased Resolution for Carbene Labeling of Protein Partners In Vitro and on Cells. *ACS Cent. Sci.* **10**, 199–208 (2024).

54. Stieger, C. E. *et al.* DFT-Guided Discovery of Ethynyl-Triazolyl-Phosphinates as Modular Electrophiles for Chemoselective Cysteine Bioconjugation and Profiling. *Angew. Chemie - Int. Ed.* **61**, (2022).

55. Toh, K. *et al.* Chemoproteomic Identification of Blue-Light-Damaged Proteins. *J. Am.*

Chem. Soc. **144**, 20171–20176 (2022).

56. Ashen-Garry, D. & Selke, M. Singlet oxygen generation by cyclometalated complexes and applications. *Photochem. Photobiol.* **90**, 257–274 (2014).

57. Insińska-Rak, M. *et al.* Spectroscopy and photophysics of flavin-related compounds: 5-deaza-riboflavin. *J. Mol. Struct.* **783**, 184–190 (2006).

58. Peraro, L. *et al.* Cell Penetration Profiling Using the Chloroalkane Penetration Assay. *J. Am. Chem. Soc.* **140**, 11360–11369 (2018).

59. Roßmann, K. *et al.* N-Methyl deuterated rhodamines for protein labelling in sensitive fluorescence microscopy. *Chem. Sci.* **13**, 8605–8617 (2022).

60. Oba, M. & Demizu, Y. *Cell-Penetrating Peptides: Design, Development and Applications*. *Cell-Penetrating Peptides: Design, Development and Applications* (Wiley-VCH Verlag, 2022). doi:10.1002/9783527835997.

61. Herce, H. D. *et al.* Cell-permeable nanobodies for targeted immunolabelling and antigen manipulation in living cells. *Nat. Chem. 2017 98* **9**, 762–771 (2017).

62. Schneider, A. F. L. L., Wallabregue, A. L. D. D., Franz, L. & Hackenberger, C. P. R. R. Targeted Subcellular Protein Delivery Using Cleavable Cyclic Cell-Penetrating Peptides. *Bioconjug. Chem.* **30**, 400–404 (2019).

63. Arafiles, J. V. V. *et al.* Cell-Surface-Retained Peptide Additives for the Cytosolic Delivery of Functional Proteins. *J. Am. Chem. Soc.* **145**, (2023).

64. Kawaguchi, Y. *et al.* Identification of cellular proteins interacting with octaarginine (R8) cell-penetrating peptide by photo-crosslinking. *Bioorganic Med. Chem. Lett.* **23**, 3738–3740 (2013).

65. Kawaguchi, Y. *et al.* Syndecan-4 Is a Receptor for Clathrin-Mediated Endocytosis of Arginine-Rich Cell-Penetrating Peptides. *Bioconjug. Chem.* **27**, 1119–1130 (2016).

66. Park, J., Koh, M., Koo, J. Y., Lee, S. & Park, S. B. Investigation of Specific Binding Proteins to Photoaffinity Linkers for Efficient Deconvolution of Target Protein. *ACS Chem. Biol.* **11**, 44–52 (2016).

67. Martin, R. M. *et al.* Principles of protein targeting to the nucleolus. *Nucleus* **6**, 314–325 (2015).

68. Jørgensen, P. L. Mechanism of the Na+, K+ pump protein structure and conformations of the pure (Na+ + K+)-ATPase. *Biochim. Biophys. Acta - Rev. Biomembr.* **694**, 27–68 (1982).

69. Kühlbrandt, W. Biology, structure and mechanism of P-type ATPases. *Nat. Rev. Mol. Cell Biol. 2004 54* **5**, 282–295 (2004).

70. Trofimenko, E. *et al.* Genetic, cellular and structural characterization of the membrane potential-dependent cell-penetrating peptide translocation pore. *Elife* **10**, (2021).

71. Gentilucci, L., Marco, R. De & Cerisoli, L. Chemical Modifications Designed to Improve Peptide Stability: Incorporation of Non-Natural Amino Acids, Pseudo-Peptide Bonds, and Cyclization. *Curr. Pharm. Des.* **16**, 3185–3203 (2010).

72. Qin, W. *et al.* Dynamic mapping of proteome trafficking within and between living cells by TransitID. *Cell* **186**, 3307-3324.e30 (2023).

73. Lee, S.-Y. Y. *et al.* Engineered allostery in light-regulated LOV-Turbo enables precise spatiotemporal control of proximity labeling in living cells. *Nat. Methods* **20**, 908–917 (2023).

74. Trojani, M. C., Santucci-Darmanin, S., Breuil, V., Carle, G. F. & Pierrefite-Carle, V. Lysosomal exocytosis: From cell protection to protumoral functions. *Cancer Lett.* **597**, 217024 (2024).

75. Ji, X., Nielsen, A. L. & Heinis, C. Cyclic Peptides for Drug Development. *Angew. Chemie Int. Ed.* **63**, e202308251 (2024).

76. Hickey, J. L., Sindhikara, D., Zultanski, S. L. & Schultz, D. M. Beyond 20 in the 21st Century: Prospects and Challenges of Non-canonical Amino Acids in Peptide Drug Discovery. *ACS Med. Chem. Lett.* **14**, 557–565 (2023).

77. Becker, T. *et al.* Transforming Chemical Proteomics Enrichment into a High-Throughput Method Using an SP2E Workflow. *JACS Au* **2**, 1712–1723 (2022).

78. Hsiao, Y. *et al.* Analysis and visualization of quantitative proteomics data using FragPipe-Analyst. doi:10.1101/2024.03.05.583643.

79. Ge, S. X., Jung, D., Jung, D. & Yao, R. ShinyGO: a graphical gene-set enrichment tool for animals and plants. *Bioinformatics* **36**, 2628–2629 (2020).